Effects of impurities on the stability of the low thermal conductivity in Fe2TiO5 ceramics

Cong Chen, Bernd Müller, Oleg Lebedev, Fabien Giovannelli, Giovanni Bruno, Fabian Delorme

Version of Record: https://www.sciencedirect.com/science/article/pii/S1044580318329309
Manuscript_4294a84e88cafe40919915d3451bce6b

Effects of impurities on the stability of the low thermal conductivity in Fe_2TiO_5 ceramics

Cong Chen[1,2*], Bernd R. Müller[2], Oleg I. Lebedev[3], Fabien Giovannelli[1], Giovanni Bruno[2,4], Fabian Delorme[1]

[1]Université de Tours, CNRS, INSA CVL, GREMAN UMR 7347, IUT de Blois, 15 rue de la chocolaterie, CS 2903, 41029 Blois Cedex, France

[2]Bundesanstalt für Materialforschung und –prüfung (BAM), Unter den Eichen 87, 12205 Berlin, Germany

[3]CRISMAT, UMR CNRS-ENSICAEN 6508, 14050 Caen, France

[4]Institute of Physics and Astronomy, University of Potsdam, Karl-Liebknecht-Str.24-25, 14476 Potsdam, Germany

* Corresponding Author. E-Mail: saracongchen@gmail.com

Abstract

The stability of the low thermal conductivity in Fe_2TiO_5 pseudobrookite ceramics has been studied. An increase in thermal diffusivity is observed after only three cycles of measurement. X-ray refraction shows an increase in the mean value of specific surface after the thermal diffusivity measurements. By using scanning electron microscopy and high-angle annular dark-field scanning transmission electron microscope equipped with energy dispersive X-ray spectroscopy, we observe a segregation of Ca- and F-rich nanocrystals at grain boundaries after three cycles of thermal diffusivity measurement. Therefore, impurities seem to be more efficient to scatter phonons as point defects in the pseudobrookite lattice rather than as nanocrystals at pseudobrookite grain boundaries. This emphasizes the importance of precursor purity and the influence of redistribution of impurities on thermoelectric properties: stability of micro-/nano-structures is a key point, and repeated thermoelectric measurements may allow detecting such metastable micro- /nano-structures and producing stable and reliable data.

Keywords:

Fe_2TiO_5; Impurity segregation; Thermoelectrics; X-ray refraction; Scanning transmission electron microscopy; Thermal conductivity

Introduction

Industrial waste heat accounts for approximately 60% of the energy input. Thermoelectric materials, capable of conversion between thermal energy and electricity, are among the best candidates to recover this enormous amount of waste heat. The conversion efficiency is determined by the temperatures at the hot and cold ends of the thermoelectric modules and by the figure of merit (ZT) of thermoelectric materials. ZT can be expressed as $ZT = S^2\sigma T/\kappa$, where S is the Seebeck coefficient, σ

is the electrical conductivity, T is the absolute temperature, and κ is the thermal conductivity. Practical applications of this technology require a ZT value higher than 1.

Various approaches have been adopted to enhance ZT such as nanostructuring [1-3], synthesizing composites [4-6] or materials with controlled porosity [7-9]. However, they all present a common issue about the thermal stability for long-term operation at high temperatures. For example, grain growth in nanostructured materials can occur at high or even at moderate temperatures, leading to the increased thermal conductivity, and therefore lower values of ZT [2, 3]. Interfacial chemical reactions between different phases in composites could also affect their mechanical properties [10]. Moreover, the pore coarsening and possible porosity reduction driven by the high initial surface area could occur in porous thermoelectric materials [11]. Furthermore, in the case of nanostructured and porous materials, the ratio of grain boundary to grain interior atoms becomes significant compared to the dense materials. The thermoelectric properties of these materials are influenced by mechanisms related to grain boundaries such as phonon-boundary scattering and energy filtering effect [1]. Therefore, the thermal stability of the grain boundaries is important for these materials. It has been found out that upon thermal cycling, impurity or dopant segregation could occur at grain boundaries, affecting grain growth kinetics [12], electrical and thermal transport properties [13-15], and mechanical properties of materials [16]. Thus, thermal stability studies are essential for the further development of the low-dimensional and porous materials.

Pseudobrookite Fe_2TiO_5 is an n-type oxide. Chen et al. have demonstrated in previous studies that it has extremely low thermal conductivity due to the presence of microcracking in the ceramics [17, 18]. The high degree of anisotropy of thermal expansion coefficient (CTE) of Fe_2TiO_5 results in the formation of residual stresses during cooling from the high-temperature sintering, which could further lead to a spontaneous microcracking. This phenomenon is common not only in pseudobrookites [19] but also in some oxides [20]. In such ceramics, the ratio of grain boundary and /or surface to grain interior is large compared to the dense ceramics, owing to microcracking. Healing and re-opening of microcracks are completely reversible under the condition of unchanged microstructure at elevated temperatures [21]. However, if the microstructure evolves, thermal expansion or diffusivity cyclic curves do not overlap [22, 23]. Therefore, it is important to investigate the thermal stability of Fe_2TiO_5 ceramics in combined terms of microstructure and microcrack density and their effect on its thermoelectric properties. In this study, we measure the thermal diffusivity of Fe_2TiO_5 for three cycles from 373 K to 1000 K and back to 373 K. The thermal diffusivity values are compared and the reasons causing the changes are examined.

The microcrack density is determined by synchrotron X-ray refraction ABI (analyzer based imaging [24]), which is well suited to the detection of defects such as pores and microcracks in materials [24-26]. This technique allows comparing the microcrack density in Fe_2TiO_5 over the heating cycles. The microstructure and chemical composition of grain boundaries in Fe_2TiO_5 ceramics are examined by

high-angle annular dark-field scanning transmission electron microscope (HAADF-STEM) equipped with energy dispersive X-ray (EDX) spectroscopy.

Experiment

Fe_2TiO_5 powder was synthesized by solid state reaction between Fe_2O_3 (Sigma Aldrich, ≥99%) and TiO_2 (Sigma Aldrich, ≥99.9%) at 1473 K for 2 h in air. The obtained powder was then sintered into pellets by conventional pressureless sintering at 1573 K for 2 h in air. The detailed synthesis method is described in Ref. [17]. The bulk density was calculated from pellet's dry mass and geometric dimensions. Coupons of approximately 6 mm × 6 mm × 1 mm were cut by a wire saw from the pellet. Phase analysis was performed by X-ray diffraction (XRD) at room temperature on both the original pellet and the coupons. A BRUKER D8 Advance θ/2θ diffractometer equipped with a Linxeye energy-dispersive one-dimensional detector was used and operated with the Cu-Kα radiation, at 40 kV and 40 mA. Scans were recorded from 10° to 80° (2θ) with a step of 0.02° and an acquisition time of 0.5 s per step. Microstructure was examined by field emission scanning electron microscopy (Tescan MIRA3). Thermal diffusivity was measured with a Netzsch LFA457 instrument over the temperature range 373 K – 1000 K upon heating and cooling in air. The heating and cooling rate was 10 $K.min^{-1}$ and it took approximately 15 minutes to stabilize the temperature at each temperature point. Three measurements were performed and each data point (at each temperature) was calculated as an average of three measurements.

X-ray refraction radiography was carried out at the synchrotron station BAMline at Helmholtz-Zentrum Berlin (HZB), Germany [27-29]. It was used to examine the porosity and relative specific surface of the coupons before and after the thermal diffusivity measurement cycles. The principle, set-up and data treatment process of the experiment can be found in Ref. [26]. For the sake of completeness, the salient information is reported here. The monochromatic photon energy was set to 30 keV by a double crystal monochromator. After interaction with the sample, the X-ray beam impinged on an analyser crystal that serves as an angular filter. Only the X-rays with an incident angle equalling the crystal's Bragg angle can be reflected to the detector. By rotating the analyser crystal in the vicinity of its Bragg angle, the so-called rocking curve was recorded for each detector pixel. The detector consisted of a Princeton Instrument camera (2048 × 2048 pixels) and a fluorescent screen of $CdWO_4$. This set-up allowed obtaining a pixel size of 3.7 µm × 3.7 µm with a field of view of 7.5 mm × 7.5 mm. The rocking curves were measured with and without specimens. Refraction properties, indicating the specific surface, are described by the so-called refraction value (C_m)

$$C_m d = 1 - \frac{I_{max}}{I_{max,\,0}} \frac{I_{int,0}}{I_{int}} \qquad (1)$$

Where d is the thickness of the specimen and I_{max} and $I_{max,\,0}$ are the rocking curve peak intensity with and without the specimen, respectively. I_{int} and $I_{int,\,0}$ are the integrated intensity of the rocking curves

with and without the specimens, respectively. X-ray transmission radiography was obtained by removing the analyser crystal from the beam. The linear attenuation coefficient (μ) is expressed as

$$\mu d = -\ln\left(\frac{I}{I_0}\right) \qquad (2)$$

Where I and I_0 are transmitted intensity and primary beam intensity, respectively. By normalizing the refraction signal to the attenuation properties, *i.e.,* by dividing $C_m d$ by μd, the influence of thickness can be eliminated. This gives the relative internal specific surface (Σ), which receives contributions from microcracks, pore surfaces, and grain boundaries.

$$\Sigma = \frac{C_m d}{\mu d} = \frac{C_m}{\mu} \qquad (3)$$

High-angle annular dark-field scanning transmission electron microscope (HAADF-STEM) and energy dispersive X-ray (EDX) spectroscopy (acquired in parallel) were performed to study the crystal structure and chemical composition of the crystalline nanoparticles grown from the surface of the coupon after three cycles of thermal diffusivity measurement. Electron microscopy was performed on JEM ARM200F cold FEG double aberration corrected microscope operated at 200kV and equipped with large angle CENTURIO EDX detector. STEM specimens were prepared by crushing the coupon in an agate mortar together with ethanol and depositing obtained suspension on Cu holey carbon grids. Crushing a sample to prepare STEM specimens allows having a reliable and statistical ensemble over a large number of nanoparticles and materials.

Results and discussion

Fig. 1 shows that pure pseudobrookite Fe_2TiO_5 with orthorhombic structure (space group *Bbmm*) has been obtained after conventional sintering. The starred impurity peaks appeared in Fig. 1b and c correspond to the modelling clay that was used to level the surface of the coupon at the X-ray focus plane. The clay was removed from the coupon with acetone and ultrasonic cleaning after XRD measurement. All diffraction peaks remain the same after three cycles of thermal diffusivity measurement, indicating no phase change during the thermal cycles. The bulk density of the pellet is 3.999 $g.cm^{-3}$, approximately 91% of its theoretical density [17].

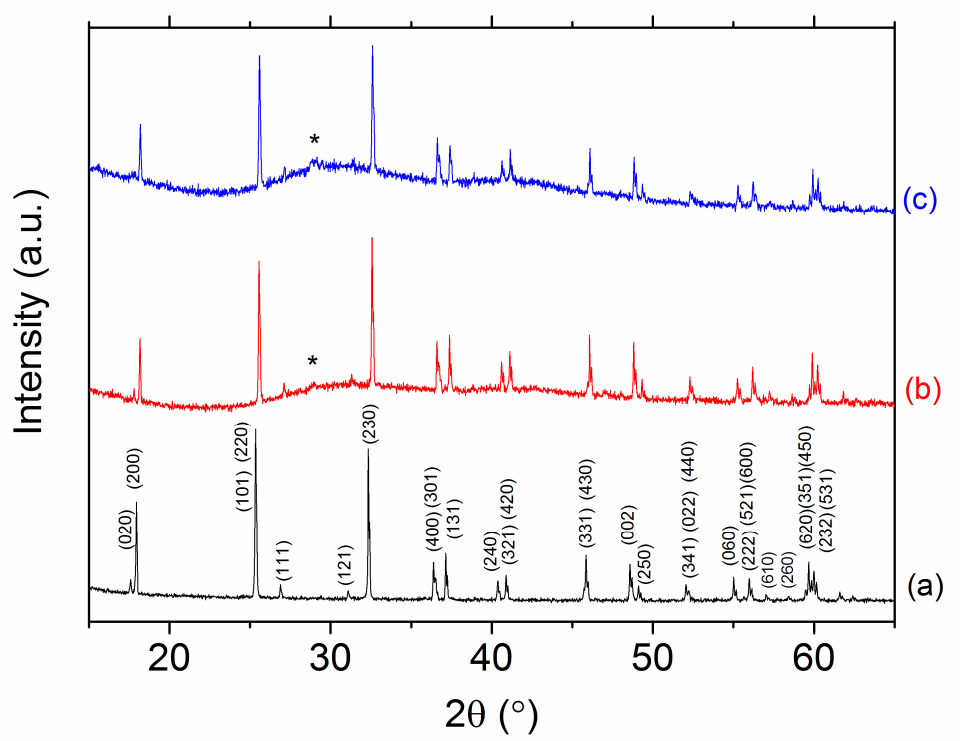

Fig. 1 X-ray diffraction pattern of Fe_2TiO_5. (a) As sintered pellet. A coupon (b) before and (c) after three cycles of thermal diffusivity measurement. The starred impurity diffraction peaks correspond to the modelling clay used to level the surface of the coupon at the X-ray focus plane.

Fig. 2a shows the temperature dependence of the thermal diffusivity of Fe_2TiO_5. During heating in each cycle, thermal diffusivity decreases with increasing temperature from 373 K to 800 K and then increases on the temperature range from 800 K to 1000 K. During cooling, thermal diffusivity further increases with decreasing temperature until 900 K, then decreases until 600 K, and finally rises again until reaching 373 K. The hysteresis in the thermal diffusivity is caused by healing and re-opening of microcracks in Fe_2TiO_5. Microcracks are induced when the Fe_2TiO_5 ceramic is cooled from the sintering temperature as a result of high anisotropy in the thermal expansion coefficient along different crystalline axes, which is typical in pseudobrookite like Fe_2TiO_5 [22], $MgTi_2O_5$ [23], and Al_2TiO_5 [30-32]. The increased thermal diffusivity above 800 K during heating marks the start of microcrack healing, while the decreased thermal diffusivity from 900 K during cooling marks the re-opening of the microcracks. Fig. 2b shows that at 373 K the thermal diffusivity increases with increasing measurement cycles, indicating the occurrence of a continuous change in the coupon. Moreover, the influence becomes moderate with increasing measurement cycles.

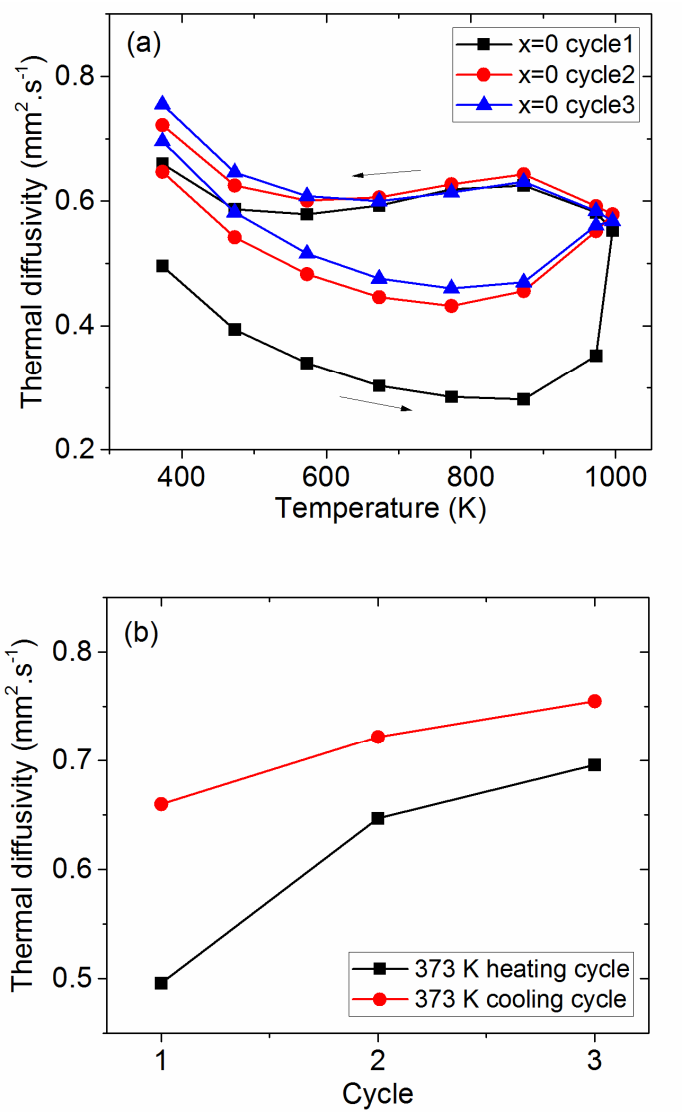

Fig. 2 Thermal diffusivity of Fe_2TiO_5 versus (a) temperature and (b) measurement cycle at 373 K. The arrows in (a) indicate the heating and cooling processes.

Fig. 3a and b show the refraction radiographs of Fe_2TiO_5 before and after three cycles of thermal diffusivity measurement, respectively. Bright areas (high grey values) indicate regions with a large relative specific surface area caused by microcracks, pore surfaces, and grain boundaries. Dark areas (low grey values) indicate areas with a small relative specific surface area. Bright and dark regions can be observed in both maps, indicating that the defects or interfaces are not homogeneously distributed in the pellet. The histogram in Fig. 3b shows a shift in the relative specific surface towards higher grey values for the coupon after three cycles of thermal diffusivity measurement, with a mean value of relative specific surface increasing from 0.235 to 0.239 (note that this change is above the error bar). This indicates a slight increase in the internal surface area, possibly due to an increased microcrack density, pore surface area and/or grain boundary density. However, as the thermal diffusivity of Fe_2TiO_5 increases with increasing number of measurement cycles, microcrack density is

unlikely to increase. Microcracks tend to reduce thermal conductivity [22]. Therefore, pore surface area and/or grain boundary density may account for the variation in the relative specific surface.

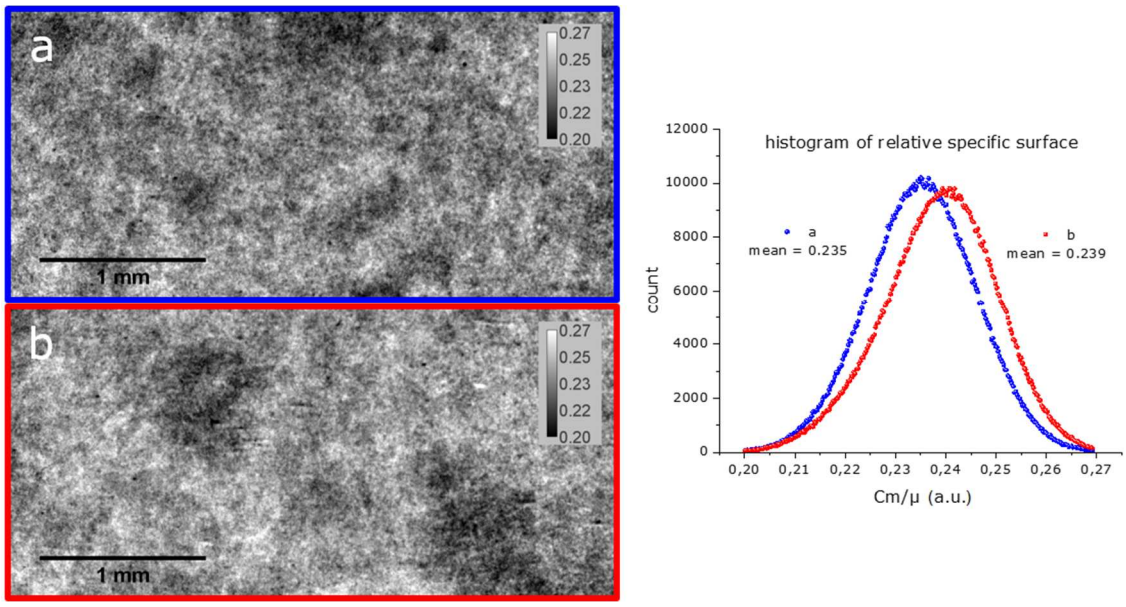

Fig. 3 2D grey scale maps of the relative specific surface C_m/μ obtained from X-ray refraction radiographs of Fe_2TiO_5 (a) before and (b) after three cycles of thermal diffusivity measurement. The grey value spread is the same for both maps. Bright areas (large grey values) indicate regions with a large relative specific surface area. Dark areas (low grey values) indicate areas with a small relative specific surface area. The histogram shows a shift towards higher grey values for the cycled coupon. The respective mean values are given beneath the graphs.

Fig. 4a and b show the microstructure of the Fe_2TiO_5 before and after three cycles of thermal diffusivity measurement. No obvious change is observed in the microstructure, regarding the grain sizes and shapes. This excludes a change in the grain boundary density during the thermal diffusivity measurements. Bright particles on the grains in both images are possibly debris from fracturing. However, a closer look at Fig. 4b reveals the presence of nanocrystals at the grain boundaries after thermal diffusivity measurements. An increase in the internal surface area is therefore due to the growth of these nanocrystals (note that the refraction signal is inversely proportional to the grain/particle/pore size). The appearance of nanocrystals also results in the evolution of the thermal diffusivity of Fe_2TiO_5. HAADF-STEM and parallel EDX mapping, which are sensitive to small changes in composition, have been carried out to confirm the phase of the crystals.

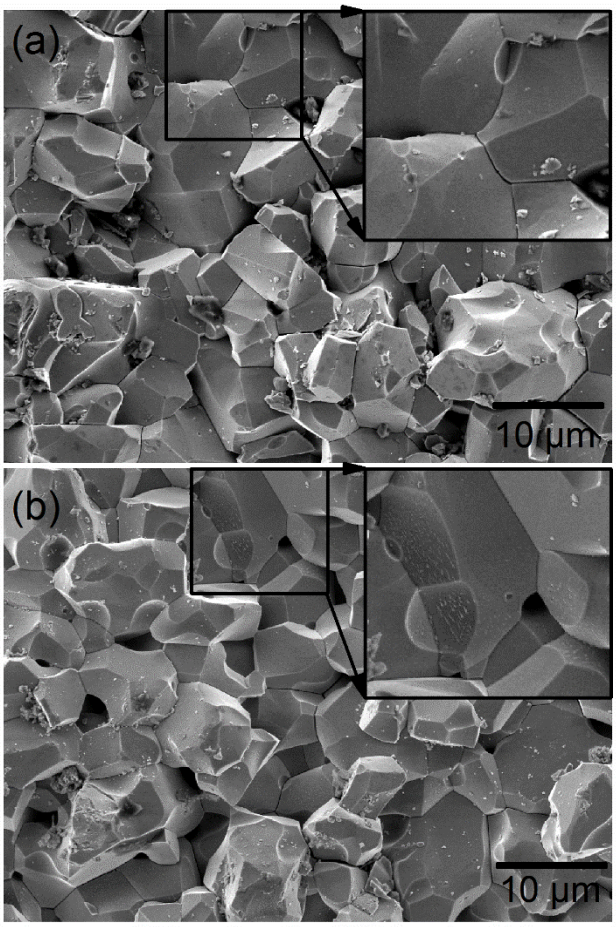

Fig. 4 SEM images of Fe_2TiO_5 (a) before and (b) after three cycles of thermal diffusivity measurement. The top right corners in both images show the magnification of the corresponding areas in the black squares.

Fig. 5 shows the HAADF-STEM images and parallel acquired EDX elemental mapping of a nanocrystal grown at the surface of Fe_2TiO_5 after three cycles of thermal diffusivity measurement. The EDX elemental mapping reveals a difference in the chemical composition between the nanocrystal and the matrix. The matrix consists of uniformly distributed Fe, Ti, Ca, F, and O, whereas the nanocrystal contains a substantial amount of Ca and a trace amount of F. The matrix phase corresponds to Fe_2TiO_5 pseudobrookite. Fig. 6 shows results of a further TEM examination of the sample. HAADF-STEM studies reveal a presence of round-shape nanoparticles with a typical size around 90 nm (Fig. 6a and b). EDX elemental mapping shows the presence of Ca, F and O within the single nanoparticle. However, Ca and F are uniformly distributed within the nanoparticle, while O is mainly located at the surface of the nanoparticle. This creates a core-shell structure with Ca-F as a core and oxide as a shell. The high resolution HAADF-STEM image and the corresponding FT pattern (Fig. 6c) reveal a cubic crystal structure, where FT pattern can be indexed as [001] view of CaF_2 structure with a space group *Fm-3m* (225) and a lattice parameter a = 5.462 Å. The presence of CaF_2 is confirmed, as (i) the EDS mapping shows that the composition of the core is 29.35 at.% of Ca

and 70.65 at.% of F and (ii) the lattice parameter of CaO (4.79 Å) is far from 5.5 Å that is determined from HR HAADF-STEM images. Calcium and fluorine come probably from impurities of the precursors, as no such elements are used in the laboratory. Moreover, SEM and EDS observations did not show the presence of secondary phases bearing these elements within the precursors. Their concentration in the bulk precursors is too low to be detected. It should be noticed that Ca is a typical impurity in metal oxides and its segregation at grain boundaries and surfaces facing pores upon annealing has also been observed in TiO_2 [33, 34]. Both the size mismatch between Ca^{2+} and Ti^{4+} or Fe^{3+} and the formation of space charge region near the interfaces drive the segregation of Ca^{2+} to the grain surfaces / boundaries. As a result, Fe_2TiO_5 with a higher purity and better crystallinity is then obtained, resulting in a higher thermal diffusivity due to the reduced phonon scattering at point defects.

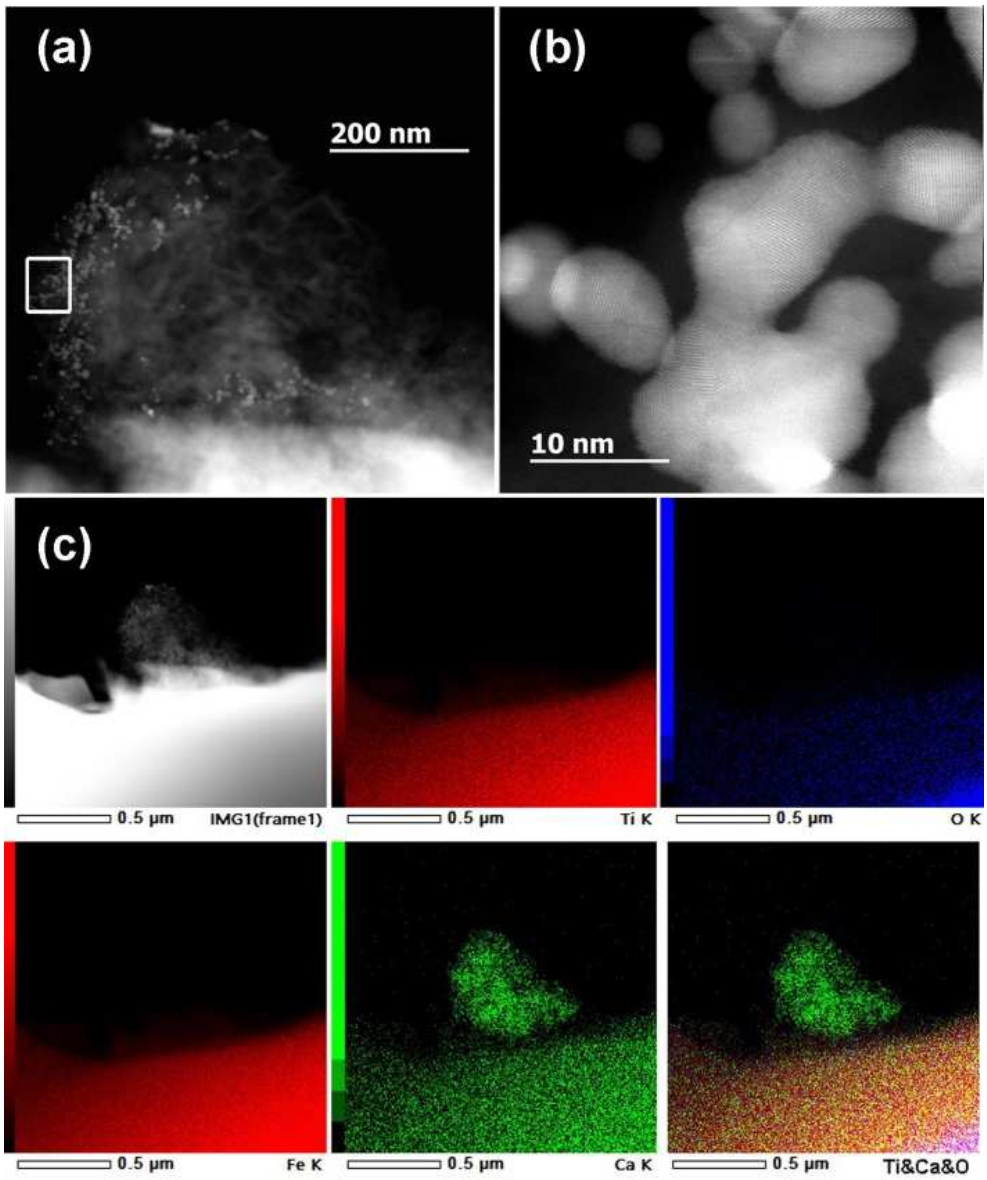

Fig. 5 (a) Low magnification HAADF-STEM image, (b) magnified HAADF-STEM image of a selected area in (a), and (c) EDX elemental mapping of Ti K, O K, Fe K and Ca K and overlaid Ti&Ca&O colored image of Fe_2TiO_5 after three cycles of thermal diffusivity measurement.

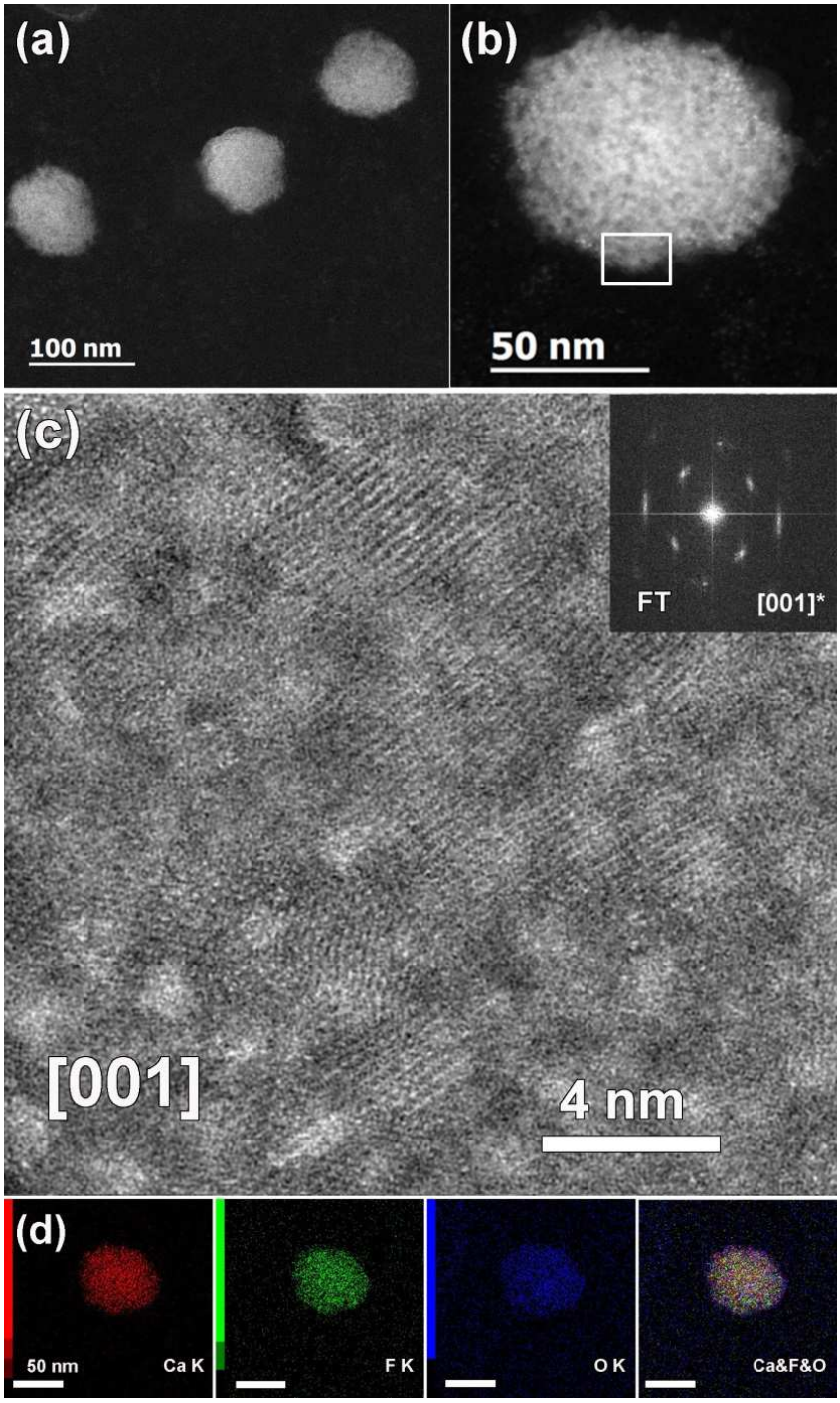

Fig. 6 (a) and (b) Low magnification HAADF-STEM images of different CaF_2 nanoparticles, (c) high resolution HAADF-STEM image of the area selected in (b), and (d) corresponding EDX elemental mapping of Ca K, F K and O K together with overlaid Ca&F&O colors.

This study gives some important implications for the development of thermoelectric materials with a high grain boundary density such as nanostructured and porous materials. First, raw materials with high-purity grade should be used for the synthesis of thermoelectric materials. Second, the redistribution of either intentionally added dopants or naturally incorporated impurities should be considered, especially for the materials with metastable microstructures such as nanostructured and porous materials, as it has a strong impact on the thermoelectric properties. Indeed, it has been clearly demonstrated that calcium and fluorine impurities were more efficient to scatter phonons as point defects in the pseudobrookite lattice rather than as nanocrystals at pseudobrookite grain boundaries. Therefore, the stability of nano/micro-structures is a key point to the stability of properties, and repeated thermoelectric measurements may be employed to ensure the stabilization of thermoelectric materials, thus allowing acquisition of stable and reliable data. Although in our study impurity segregation appears less efficient than point defects, it may have the potential for improving thermoelectric properties in other compounds through enhanced phonon scattering [35] or increased carrier mobility [15, 36].

Conclusion

We have observed (by SEM and HAADF-STEM-EDX) the segregation of Ca- and F-rich nanocrystals at the grain boundaries of Fe_2TiO_5 pseudobrookite after three cycles of thermal diffusivity measurement. Segregation of nanocrystals results in an increase of thermal diffusivity with increasing number of measurement cycles. Therefore, the Ca and F impurities seems to be more efficient to scatter phonons as point defects in the pseudobrookite lattice rather than as nanocrystals at pseudobrookite grain boundaries. They also lead to an increase in the relative specific surface of Fe_2TiO_5 as confirmed by X-ray refraction. The present work shows that redistribution of impurities can have a great influence on thermoelectric properties, particularly for the materials with metastable microstructures such as nanostructured and porous materials. Repeated thermoelectric measurements may allow detecting such metastable nano/micro-structures and producing stable and reliable data. Furthermore, X-ray refraction can detect features of nanometric size (1 nm) but still give quantitative analyses over a large field of view. It complements the microscopic characterization techniques such as SEM and TEM.

Acknowledgements

C. Chen, O.I. Lebedev, F. Giovannelli, and F. Delorme are grateful to the French METSA network (FR3507) for its financial support.

Data availability

The authors confirm that the data supporting the findings of this study are available within the article.

References

1. Dresselhaus, M.S., G. Chen, M.Y. Tang, R.G. Yang, H. Lee, D.Z. Wang, Z.F. Ren, J.P. Fleurial, and P. Gogna, *New directions for low - dimensional thermoelectric materials.* Adv. Mater., 2007. **19**(8): p. 1043-1053.
2. Giovannelli, F., C. Chen, P. Díaz-Chao, E. Guilmeau, and F. Delorme, *Thermal conductivity and stability of Al-doped ZnO nanostructured ceramics.* J. Eur. Ceram. Soc., 2018. **38**(15): p. 5015-5020.
3. Kanatzidis, M.G., *Nanostructured Thermoelectrics: The New Paradigm?* Chem. Mater., 2010. **22**(3): p. 648-659.
4. Wang, N., H. Chen, H. He, W. Norimatsu, M. Kusunoki, and K. Koumoto, *Enhanced thermoelectric performance of Nb-doped $SrTiO_3$ by nano-inclusion with low thermal conductivity.* Sci. Rep., 2013. **3**: p. 3449.
5. Chen, C., T. Zhang, R. Donelson, D. Chu, R. Tian, T.T. Tan, and S. Li, *Thermopower and chemical stability of $Na_{0.77}CoO_2/Ca_3Co_4O_9$ composites.* Acta Mater., 2014. **63**: p. 99-106.
6. Delorme, F., P. Diaz-Chao, E. Guilmeau, and F. Giovannelli, *Thermoelectric properties of $Ca_3Co_4O_9$–Co_3O_4 composites.* Ceramics International, 2015. **41**(8): p. 10038-10043.
7. Kashiwagi, M., S. Hirata, K. Harada, Y. Zheng, K. Miyazaki, M. Yahiro, and C. Adachi, *Enhanced figure of merit of a porous thin film of bismuth antimony telluride.* Appl. Phys. Lett., 2011. **98**(2): p. 023114.
8. Ju, H., K. Kim, D. Park, and J. Kim, *Fabrication of porous SnSeS nanosheets with controlled porosity and their enhanced thermoelectric performance.* Chem. Eng. J., 2018. **335**: p. 560-566.
9. Wu, C.F., T.R. Wei, F.H. Sun, and J.F. Li, *Nanoporous PbSe–SiO_2 Thermoelectric Composites.* Advanced Science, 2017. **4**(11): p. 1700199.
10. Ci, L., Z. Ryu, N.Y. Jin-Phillipp, and M. Rühle, *Investigation of the interfacial reaction between multi-walled carbon nanotubes and aluminum.* Acta Mater., 2006. **54**(20): p. 5367-5375.
11. Kumar, K.N.P., J. Tranto, J. Kumar, and J.E. Engell, *Pore-structure stability and phase transformation in pure and M-doped (M=La, Ce, Nd, Gd, Cu, Fe) alumina membranes and catalyst supports.* Journal of Materials Science Letters, 1996. **15**(3): p. 266-270.
12. Chung, S.-Y., S.-J.L. Kang, and V.P. Dravid, *Effect of Sintering Atmosphere on Grain Boundary Segregation and Grain Growth in Niobium-Doped $SrTiO_3$.* J. Am. Ceram. Soc., 2002. **85**(11): p. 2805-2810.
13. Demetry, C. and X. Shi, *Grain size-dependent electrical properties of rutile (TiO_2).* Solid State Ionics, 1999. **118**(3): p. 271-279.
14. Gambaryan-Roisman, T., E.Y.A. Litovsky, M. Shapiro, and A. Shavit, *Effect of surface segregation kinetics on the effective thermal conductivity of porous ceramics.* International Journal of Heat and Mass Transfer, 1996. **39**(8): p. 1687-1695.
15. Boyle, C., P. Carvillo, Y. Chen, E.J. Barbero, D. McIntyre, and X. Song, *Grain boundary segregation and thermoelectric performance enhancement of bismuth doped calcium cobaltite.* J. Eur. Ceram. Soc., 2016. **36**(3): p. 601-607.
16. Cook, R.F. and A.G. Schrott, *Calcium segregation to grain boundaries in alumina.* J. Am. Ceram. Soc., 1988. **71**(1): p. 50-58.
17. Chen, C., F. Giovannelli, J.-R. Duclère, and F. Delorme, *Thermoelectric properties of $Fe_2(Ti_{1-x}Nb_x)O_5$ pseudobrookite ceramics with low thermal conductivity.* J. Eur. Ceram. Soc., 2017. **37**(15): p. 4681-4685.
18. Chen, C., F. Giovannelli, and F. Delorme, *Thermoelectric properties of $Fe_{2-x}Ti_{1+x}O_5$ solid solutions: Influence of microcracking and Nb substitution.* Ceram. Int., 2018. **44**(17): p. 21794-21799.
19. TVERGAARD, V. and J.W. HUTCHINSON, *Microcracking in ceramics induced by thermal expansion or elastic anisotropy.* J. Am. Ceram. Soc., 1988. **71**(3): p. 157-166.
20. Bruno, G., A.M. Efremov, B. Clausen, A.M. Balagurov, V.N. Simkin, B.R. Wheaton, J.E. Webb, and D.W. Brown, *On the stress-free lattice expansion of porous cordierite.* Acta Mater., 2010. **58**(6): p. 1994-2003.

21. Bruno, G., A.M. Efremov, C. An, and S. Nickerson, *Not all microcracks are born equal: thermal vs. mechanical microcracking in porous ceramics*, in *Advances in Bioceramics and Porous Ceramics IV*, P.C. R. Narayan, S. Widjaja and D. Singh, Editor. 2011.
22. Siebeneck, H.J., D.P.H. Hasselman, J.J. Cleveland, and R.C. Bradt, *Effect of microcracking on the thermal diffusivity of Fe_2TiO_5.* J. Am. Ceram. Soc., 1976. **59**(5 - 6): p. 241-244.
23. Siebeneck, H.J., D.P.H. Hasselman, J.J. Cleveland, and R.C. Bradt, *Effects of grain size and microcracking on the thermal diffusivity of $MgTi_2O_5$.* J. Am. Ceram. Soc., 1977. **60**(7 - 8): p. 336-338.
24. Nellesen, J., R. Laquai, B.R. Müller, A. Kupsch, M.P. Hentschel, N.B. Anar, E. Soppa, W. Tillmann, and G. Bruno, *In situ analysis of damage evolution in an Al/ Al_2O_3 MMC under tensile load by synchrotron X-ray refraction imaging.* Journal of Materials Science, 2018. **53**(8): p. 6021-6032.
25. Kupsch, A., B.R. Müller, A. Lange, and G. Bruno, *Microstructure characterisation of ceramics via 2D and 3D X-ray refraction techniques.* J. Eur. Ceram. Soc., 2017. **37**(5): p. 1879-1889.
26. Müller, B.R., R.C. Cooper, A. Lange, A. Kupsch, M. Wheeler, M.P. Hentschel, A. Staude, A. Pandey, A. Shyam, and G. Bruno, *Stress-induced microcrack density evolution in β-eucryptite ceramics: Experimental observations and possible route to strain hardening.* Acta Mater., 2018. **144**: p. 627-641.
27. Görner, W., M.P. Hentschel, B.R. Müller, H. Riesemeier, M. Krumrey, G. Ulm, W. Diete, U. Klein, and R. Frahm, *BAMline: the first hard X-ray beamline at BESSY II.* Nuclear Instruments and Methods in Physics Research Section A: Accelerators, Spectrometers, Detectors and Associated Equipment, 2001. **467-468**: p. 703-706.
28. Riesemeier, H., K. Ecker, W. Görner, B.R. Müller, M. Radtke, and M. Krumrey, *Layout and first XRF applications of the BAMline at BESSY II.* X-Ray Spectrometry, 2005. **34**(2): p. 160-163.
29. Rack, A., H. Riesemeier, S. Zabler, T. Weitkamp, B.R. Müller, G. Weidemann, P. Modregger, J. Banhart, L. Helfen, A.N. Danilewsky, H.G. Gräber, R. Heldele, B. Mayzel, J. Goebbels, and T. Baumbach. *The high-resolution synchrotron-based imaging stations at the BAMline (BESSY) and TopoTomo (ANKA).* in *Optical Engineering + Applications*. 2008. SPIE.
30. Chen, C.-H. and H. Awaji, *Temperature dependence of mechanical properties of aluminum titanate ceramics.* J. Eur. Ceram. Soc., 2007. **27**(1): p. 13-18.
31. Bruno, G., A. Efremov, B. Wheaton, I. Bobrikov, V.G. Simkin, and S. Misture, *Micro- and macroscopic thermal expansion of stabilized aluminum titanate.* J. Eur. Ceram. Soc., 2010. **30**(12): p. 2555-2562.
32. Bruno, G., A.M. Efremov, B.R. Wheaton, and J.E. Webb, *Microcrack orientation in porous aluminum titanate.* Acta Mater., 2010. **58**(20): p. 6649-6655.
33. Zhang, L.P., M. Li, and U. Diebold, *Characterization of Ca impurity segregation on the TiO_2(110) surface.* Surface Science, 1998. **412-413**: p. 242-251.
34. Dulub, O., C.D. Valentin, A. Selloni, and U. Diebold, *Structure, defects, and impurities at the rutile TiO_2(011)-(2×1) surface: A scanning tunneling microscopy study.* Surface Science, 2006. **600**(19): p. 4407-4417.
35. Zeier, W.G., A. LaLonde, Z.M. Gibbs, C.P. Heinrich, M. Panthöfer, G.J. Snyder, and W. Tremel, *Influence of a nano phase segregation on the thermoelectric properties of the p-Type doped stannite compound $Cu_{2+x}Zn_{1-x}GeSe_4$.* J. Am. Chem. Soc., 2012. **134**(16): p. 7147-7154.
36. Carvillo, P., Y. Chen, C. Boyle, P.N. Barnes, and X. Song, *Thermoelectric performance enhancement of calcium cobaltite through barium grain boundary segregation.* Inorganic Chemistry, 2015. **54**(18): p. 9027-9032.